Magnetic field correlations in kinematic two-dimensional magnetohydrodynamic turbulence

Jörg Schumacher and Bruno Eckhardt
Fachbereich Physik, Philipps-Universität Marburg, D-35032 Marburg, Germany
(November 1999)

The scaling properties of the second order magnetic structure function $D_2^{(B)}(r)$ and the corresponding magnetic correlation function $C_2^{(B)}(r)$ are derived for two-dimensional magnetohydrodynamic turbulence in the kinematic regime where the ratio of kinetic energy to magnetic energy is much larger than one. In this regime the magnetic flux function ψ can be treated as a passive scalar advected in a two-dimensional turbulent flow. Its structure function $D_2^{(\psi)}(r)$ and the one for the magnetic field $D_2^{(B)}(r)$ are connected by an exact relation. We calculate $D_2^{(\psi)}(r)$ and thus $D_2^{(B)}(r)$ within geometric measure theory over a wide range of scales r and magnetic Prandtl numbers Pr_m. The magnetic field correlations follow a $r^{-4/3}$–scaling law and show an anticorrelation at the beginning of the Batchelor regime indicative of the formation of strongly filamented current sheets. Differences to the full dynamic regime, where the ratio of kinetic to magnetic energies is smaller than in the kinematic case, are discussed.

arXiv:chao-dyn/9904014v2 8 Nov 1999

I. INTRODUCTION

Magnetohydrodynamic (MHD) turbulence appears in many problems in nuclear fusion research as well as in astrophysics and geophysics (see, e.g. Refs. 1 and 2 for reviews). Compared to the already complicated hydrodynamic turbulence there are additional degrees of complexity due to the presence of a magnetic field, the possibility of dynamos and the action of the magnetic field back on the flow through the Lorentz force. In addition, the distribution of energy among the modes is controlled through the interaction of three cascade processes, related to the three conserved quantities of the dynamical equations in the inviscid limit: the total energy, the cross helicity, and for two dimensions the mean square magnetic potential. There is, however, a regime where some of the more complicated processes are subdominant or absent and where a rather complete analysis can be performed: two-dimensional (2-D) magnetohydrodynamics with weak magnetic fields. This regime can be relevant to astrophysical applications, such as quasi-two-dimensional turbulent processes in thin accretion discs. [3]

The situation we consider is that of a 2-D turbulent flow, maintained by some external force, in which a magnetic field is advected. The linearity of the equation for the magnetic induction implies that without an external seed field no magnetic field will ever be generated. Moreover, the absence of dynamo action in two dimensions [4] implies that without permanent driving the magnetic field will die out eventually. The action of the magnetic field back on the flow can be neglected if the Lorentz force is sufficiently weak, i.e., if the magnetic field is sufficiently small. Because of the absence of dynamos in 2-D the amplitude of the external driving controls the magnitude of the magnetic field. We thus have a regime of kinematic evolution of a magnetic field passively advected by the turbulent flow which can be realized in any 2-D situation for sufficiently small driving of the magnetic field.

The dynamics of the magnetic field and thus its correlation functions are nevertheless nontrivial since a transient growth and the development of fractal like structures on small scales are possible, as evidenced by numerical simulations. [5,6] Though the range of applicability of this kinematic approach is limited, it shows some interesting features which we would like to describe here.

On a technical level, the restriction to a 2-D situation allows to connect the evolution of the vector potential to that of a scalar field for which detailed scaling predictions exist within geometric measure theory. [7–9] On the assumptions of statistical stationarity, homogeneity, and isotropy for both the magnetic field and the scalar field, geometric measure theory provides a connection between the structure functions of the velocity field and the scalar field. In particular, the scaling behavior can be related and the dependence on the Prandtl number and on another parameter that characterizes the strength of the driving and appears in 2-D only can be extracted. Using an exact relation between the correlation function of the scalar and the magnetic field we can transfer these results to the magnetohydrodynamic problem and in particular discuss the dependence on the magnetic Prandtl number. The latter can range from $Pr_m \sim 10^{-6}$ in the solar convection zone to $Pr_m \sim 10^7$ in the interstellar medium. [10] Within the kinematic regime we are able to go beyond previous applications of geometric measure theory to MHD turbulence. [11,12]

The outline of the paper is as follows. In sections II and III the theoretical background in 2-D magnetohydrodynamics and 2-D passive scalar advection is summarized. For details on the analysis of the 2-D passive scalar within geometric measure theory we refer to our previous work. [9] In section IV both are combined and the correlation and structure functions of magnetic fields in the kinematic regime are discussed. In section V we compare with correlation functions and structure functions found in full numerical simulations; this highlights features of the interaction between both fields which have

to be included when the magnetic field becomes dynamically relevant. We conclude with a summary in section VI.

II. MHD BASICS

The equations for a magnetic field $\mathbf{B}(\mathbf{x},t)$ in a conducting fluid moving with velocity $\mathbf{u}(\mathbf{x},t)$ are

$$\rho\left(\partial_t\mathbf{u}+(\mathbf{u}\cdot\nabla)\mathbf{u}\right) = -\nabla p+\frac{1}{\mu_0}(\nabla\times\mathbf{B})\times\mathbf{B}+\rho\nu\Delta\mathbf{u}+\rho\mathbf{f}_u \tag{1}$$

$$\partial_t\mathbf{B}+(\mathbf{u}\cdot\nabla)\mathbf{B} = (\mathbf{B}\cdot\nabla)\mathbf{u}+\eta\Delta\mathbf{B}+\mathbf{f}_B \tag{2}$$

$$\nabla\cdot\mathbf{u}=\nabla\cdot\mathbf{B}=0 \tag{3}$$

where ν is the kinematic viscosity, η is magnetic diffusivity, p is the thermal pressure, and $\mathbf{f}_u$ and $\mathbf{f}_B$ are the external driving for each field. The quantity ρ is the constant mass density and μ_0 denotes the permeability in a vacuum. We estimate typical amplitudes for the velocity field and the magnetic field by the root mean square values $u_{r.m.s.}=\langle u_x^2\rangle^{1/2}$ and $B_{r.m.s.}=\langle B_x^2\rangle^{1/2}$ where $\langle\cdot\rangle$ denotes a statistical average over an isotropic and homogeneous ensemble. If then L is an external length scale, the fluid Reynolds number $R=u_{r.m.s.}L/\nu$ and the magnetic Reynolds number $R_m=u_{r.m.s.}L/\eta$ can be formed. Their ratio defines the magnetic Prandtl number $Pr_m=\nu/\eta=R_m/R$. The relative size of magnetic field and velocity field is measured by the Alfvén-Mach number M, the ratio of the typical fluid velocity $u_{r.m.s.}$ to the Alfvén velocity $v_A=B_{r.m.s.}/(\mu_0\rho)^{1/2}$,

$$\begin{aligned} M &= \frac{u_{r.m.s.}}{v_A}, \\ &= \left(\frac{\mu_0\rho u_{r.m.s.}^2}{B_{r.m.s.}^2}\right)^{1/2}, \\ &= \left(\frac{E_K}{E_B}\right)^{1/2}. \end{aligned} \tag{4}$$

By the last line this is also the square root of the ratio between fluid kinetic energy and magnetic field energy.

With these definitions, the dimensionless form of the first two equations reads

$$\partial_t\mathbf{u}+(\mathbf{u}\cdot\nabla)\mathbf{u} = -\nabla p+M^{-2}(\nabla\times\mathbf{B})\times\mathbf{B}+R^{-1}\Delta\mathbf{u}+\mathbf{f}_u \tag{5}$$

$$\partial_t\mathbf{B}+(\mathbf{u}\cdot\nabla)\mathbf{B} = (\mathbf{B}\cdot\nabla)\mathbf{u}+R_m^{-1}\Delta\mathbf{B}+\mathbf{f}_B\,. \tag{6}$$

In two dimensions, both the velocity field and the magnetic field can be represented by scalar fields by introducing the vorticity

$$\omega\mathbf{e}_z=\nabla\times\mathbf{u}\,, \tag{7}$$

and the magnetic flux function

$$\mathbf{B}=\nabla\psi\times\mathbf{e}_z\,. \tag{8}$$

The MHD equations then take on the form

$$\partial_t\omega+(\mathbf{u}\cdot\nabla)\omega = M^{-2}(\mathbf{B}\cdot\nabla)j+R^{-1}\nabla^2\omega+f_\omega\,, \tag{9}$$

$$\partial_t\psi+(\mathbf{u}\cdot\nabla)\psi = R_m^{-1}\nabla^2\psi+f_\psi\,, \tag{10}$$

with $j=-\nabla^2\psi$ the z-component of the current density and f_ψ and f_ω the scalar driving fields .

The situation we want to consider is one of weak magnetic fields, i.e. very large M, so that the term with the Lorentz force density can be ignored. This can be estimated to be reasonable [5] if the Mach number exceeds the magnetic Reynolds number, i.e. if $M>R_m$. Then the equations for the fluid do not depend on the magnetic field any more and the statistically stationary state that develops depends only on the strength of the force f_ω and the length scale l_f on which it acts. In 2-D turbulence it is the enstrophy that cascades down to the viscous scales. So if we assume homogeneity and isotropy the appropriate smallest scale is the enstrophy dissipation length $\eta_\omega=\nu^{1/2}\epsilon_\omega^{-1/6}$, defined in terms of the enstrophy dissipation rate $\epsilon_\omega=\nu\langle|\nabla\omega|^2\rangle$.

The quantities we want to study are the second order structure function $D_2^{(B)}(r)$,

$$D_2^{(B)}(r)=\langle|\mathbf{B}(\mathbf{x}+\mathbf{r})-\mathbf{B}(\mathbf{x})|^2\rangle\,, \tag{11}$$

and the correlation function $C_2^{(B)}(r)$,

$$C_2^{(B)}(r)=\langle\mathbf{B}(\mathbf{x}+\mathbf{r})\cdot\mathbf{B}(\mathbf{x})\rangle\,, \tag{12}$$

of the magnetic field. $D_2^{(B)}(r)$ and $C_2^{(B)}(r)$ are related by

$$D_2^{(B)}(r)=2\langle B^2\rangle-2C_2^{(B)}(r)\,. \tag{13}$$

Continuity of the fields on small scales and decay of correlations on large scales implies the following limiting behavior for small and large distances r:

$$D_2^{(B)}(r)=\begin{cases}\epsilon_B r^2/(2\eta)\to 0 & :\ r\to 0\\ 2\langle B^2\rangle & :\ r\to L\,,\end{cases} \tag{14}$$

whereas it is the other way round for the correlation function,

$$C_2^{(B)}(r) = \begin{cases} 2\langle B^2\rangle & : \ r \to 0 \\ 0 & : \ r \to L \, . \end{cases} \tag{15}$$

Similar quantities can be defined for the velocity field and the magnetic flux function ψ. The quantity $\epsilon_B = \eta\langle|\nabla\mathbf{B}|^2\rangle$ is the magnetic energy dissipation rate. Since ψ obeys in the kinematic limit the equations of a passive scalar, we can use our previous results for the scaling of a passive scalar in a turbulent fluid to obtain the scaling regimes for ψ. They can be transfered to the magnetic field case by use of the relations [13] (see Appendix A for the derivation)

$$D_2^{(B)}(r) = 2\frac{\epsilon_\psi}{\eta} - \Delta D_2^{(\psi)}(r), \tag{16}$$

and consequently with (13)

$$C_2^{(B)}(r) = \frac{1}{2}\Delta D_2^{(\psi)}(r). \tag{17}$$

The quantity $\epsilon_\psi = \eta\langle|\nabla\psi|^2\rangle = \eta\langle B^2\rangle$ is the mean flux dissipation rate.

III. 2-D PASSIVE SCALAR ADVECTION

In the limit of large M the magnetic flux ψ does not act on the flow field $\mathbf{u}$, so that (10) describes the passive advection of a scalar field in the velocity field that follows from the hydrodynamic driving. A connection between the scaling behavior of the fluid, as contained in the velocity structure function,

$$D_2(r) = \langle|\mathbf{u}(\mathbf{x}+\mathbf{r}) - \mathbf{u}(\mathbf{x})|^2\rangle \, , \tag{18}$$

and its longitudinal part,

$$D_\parallel(r) = \frac{1}{r^2}\int_0^r \rho \, D_2(\rho) \, \mathrm{d}\, \rho \, , \tag{19}$$

and the scaling behavior of the second order scalar field structure function,

$$\begin{aligned} D_2^{(\psi)}(r) &= \langle|\psi(\mathbf{x}+\mathbf{r}) - \psi(\mathbf{x})|^2\rangle \, , \\ &\propto r^{\zeta_2^{(\psi)}} \, , \end{aligned} \tag{20}$$

can be found within geometric measure theory. [7,8] One estimates the fractal dimension $\delta_g^{(1)}$ of level sets $\psi_0 = \psi(\mathbf{x})$ of the scalar field graph $G = (\mathbf{x}, \psi(\mathbf{x}))$, and obtains in the absence of intermittency corrections, i.e. $\zeta_2^{(\psi)} = 2\zeta_1^{(\psi)}$, the upper bound

$$2\delta_g^{(1)} \le 4 - \zeta_2^{(\psi)} \, . \tag{21}$$

Building on Ref. 7 and extending the results of Ref. 8 we were able to obtain scale resolved and Prandtl number dependent upper bounds for $\delta_g^{(1)}$, which turned out to be rather sharp. [9] If we assume that the bounds on $\delta_g^{(1)}$ are indeed equalities, (21) gives an upper bound on $\zeta_2^{(\psi)}$, viz.

$$\zeta_2^{(\psi)} = 2 - 2\frac{\mathrm{d}}{\mathrm{d}\,\ln r}\ln\sqrt{1 + \alpha\, Pr_m\, r^2 + \sqrt{3} Pr_m r\sqrt{D_\parallel}} \, . \tag{22}$$

In the following we will evaluate the right hand side and in particular its dependence on the scaling of the velocity field and take this as an estimate for the scaling exponent $\zeta_2^{(\psi)}$. As mentioned, this relies on the assumption that several inequalites are in fact equalities and that intermittency effects are absent. A careful analysis of the derivation shows that the presence of intermittency in the scalar field modifies several approximations and that the cumulative effect is difficult to control. It is fairly straightforward, however, to allow for intermittency effects in the velocity structure function.

The dimensionless parameter $\alpha = \epsilon_\psi/(\epsilon_\omega^{1/3}\psi_{r.m.s.}^2)$ measures the ratio of the scalar driving rate $\epsilon_\psi/\psi_{r.m.s.}^2$ to the flow advection rate $\epsilon_\omega^{1/3}$ and is specific to two-dimensional passive scalar advection. For large values of α the scalar cannot be advected sufficiently rapidly to the small dissipative scales so that a space filling distribution with $\zeta_2^{(\psi)} = 0$ develops. The distance r is measured in units of η_ω and the longitudinal structure function $D_\parallel(r)$ of the velocity field is measured in units of $\epsilon_\omega^{2/3}\eta_\omega^2$. The explicit dependence on the longitudinal velocity structure function $D_\parallel$ allows to substitute numerical or experimental findings for the velocity structure function, which very often differ from theoretical expectations, and to obtain predictions for the corresponding scalar structure functions.

As in the previous work [9] we use in particular structure functions obtained from Fourier transforms of model spectra in k-space and evaluate (22) numerically. Recent experiments on forced two-dimensional turbulence [14,15] and a number of direct numerical simulations [16–18] support the existence of a Kolmogorov-like scaling for the energy spectrum, $E(k) \sim k^{-5/3}$ in the inverse energy inertial subrange $k < k_f$ and a scaling $E(k) \sim k^{-\beta}$ with $\beta \ge 3$ for the direct enstrophy inertial subrange $k > k_f$. Recent experiments on 2-D turbulence indicate that the velocity increments in both cascade regimes show a non-intermittent Gaussian behavior. [14,19] We do not discuss here the role of coherent, large scale vortices which are formed by the inverse energy cascade in two-dimensional hydrodynamic turbulence and which can effect the spectra in the enstrophy subrange. This problem is still a matter of debate. [20,21] We therefore take for our analysis the following model spectrum for the amplitudes $\langle|\mathbf{u_k}|^2\rangle$ of the velocity field in a Fourier representation in a periodic box of size $L = 2\pi$:

$$\langle|\mathbf{u_k}|^2\rangle \sim \begin{cases} k_f^{-7/3} k_1^{-11/3} k^3 & : \quad \frac{2\pi}{L} \le k \le k_1, \\ k_f^{-7/3} k^{-2/3} & : \quad k_1 < k \le k_f, \\ k^{-3} & : \quad k_f < k \le k_\omega = \frac{1}{\eta_\omega}, \\ k^{-3} \exp\left[-\left(\frac{k-k_\omega}{k_\omega}\right)^2\right] & : \quad k_\omega < k\ . \end{cases} \tag{23}$$

Note the differences in scaling between the amplitudes $\langle|\mathbf{u_k}|^2\rangle$ and the energy spectrum $E(k)$ due to phase space factor, i.e. $E(k) \sim k^{-\beta-1}$ corresponds to $\langle|\mathbf{u_k}|^2\rangle \sim k^{-\beta}$. For a dependence of the results on β the reader is refered to our previous work, where we showed that a variation of β in a range between 2 and 4 left the scaling of $D_2(r)$ in the enstrophy intertial subrange nearly unchanged. We therefore take the exponent $\beta = 3$ for $\langle|\mathbf{u_k}|^2\rangle$ [see Eq. (23)] in all calculations here.

Assuming stationarity, homogeneity, and isotropy the relation between velocity spectrum scaling and the velocity structure function $D_2(r)$ is given by the volume average

$$\begin{aligned} D_2(r) &= \frac{1}{V}\int_V |\,\mathbf{u}(\mathbf{x}+\mathbf{r}) - \mathbf{u}(\mathbf{x})\,|^2\,\mathrm{d}V, \\ &= \frac{1}{V}\int_V |\sum_{\mathbf{k}} \mathbf{u_k}\,\exp(i\mathbf{k}\cdot\mathbf{x})[\exp(i\mathbf{k}\cdot\mathbf{r}) - 1]\,|^2\,\mathrm{d}V, \\ &= 2\sum_{\mathbf{k}} \langle|\mathbf{u_k}|^2\rangle\,(1 - \cos(\mathbf{k}\cdot\mathbf{r}))\,. \end{aligned} \tag{24}$$

By averaging over all directions (due to isotropy) in $\mathbf{k}$-space the cosine gives rise to the Bessel function $\mathrm{J}_0(kr)$,

$$D_2(r) = 2\sum_k \langle|\mathbf{u_k}|^2\rangle\,(1 - \mathrm{J}_0(kr))\,. \tag{25}$$

The model spectrum (23) is then substituted and the summation in (25) is evaluated numerically using a finite set of wave numbers, equidistant on a logarithmic scale. We checked the independence of our results for several wavenumber resolutions .

The algebraic scaling of $D_2(r)$ with respect to r is shown in Fig. 1 (thick dash-dotted line). For the dissipation scales $r < \eta_\omega$ it follows a r^2–dependence in correspondence with the Taylor expansion. This quadratic scaling with respect to r continues in the enstrophy inertial subrange for scales $\eta_\omega < r < l_f$. For distances $l_f < r$ the energy inertial subrange with a $r^{2/3}$–scaling sets in. Finally, a saturation to a constant value due to finite size effects is observed.

IV. 2-D KINEMATIC MHD TURBULENCE

Using the energy spectra (23) we can now evaluate the passive scalar structure and correlation function exponents and, via (16), the corresponding behavior for the magnetic fields. The results for a large range of length scales and magnetic Prandtl numbers are shown in Figs. 1 and 2. The structure function is plotted in units of $\epsilon_\psi \epsilon_\omega^{-1/3}$, and $\log_{10} D_2^{(\psi)}$ is obtained by numerical integration of $\zeta_2^{(\psi)}(r)$ over $\log_{10} r$. We find in both figures the following scaling regimes. For small scales $r < \eta_\omega$ the fields are smooth and one finds $D_2^{(\psi)}(r) = (\epsilon_\psi/2\eta) r^2$ and thus $\zeta_2^{(\psi)} = 2$. The quadratic scaling continues into the enstrophy inertial subrange $r \gtrsim \eta_\omega$. For sufficiently large Pr_m the third term under the square root in Eq. (22) gives the dominant contributions and the scaling exponent changes to $\zeta_2^{(\psi)} = 0$; this is the viscous–convective Batchelor regime [22]. The flux ψ is then advected chaotically in a velocity field that is still smooth on these scales, i.e. $D_\parallel \sim r^2$ and the flux contours are stretched and twisted by the fluid motion and form filamented current sheets. The $r^{2/3}$–scaling regime for larger r and for both the velocity field and the magnetic flux function is connected with the inverse cascade of the underlying fluid turbulence; this is the inertial–convective Obukhov–Corrsin regime [23]. The final saturation to a constant value for very large separations is due to the finite system size L.

The scaling of the structure function $D_2^{(B)}(r)$ as well as of the correlation function $C_2^{(B)}(r)$ follow from Eqns. (16) and (17), respectively. The results for the structure function of the magnetic field $D_2^{(B)}(r)$ in units of $\epsilon_\psi \nu^{-1}$ are shown in Fig. 3 (thick solid lines). Clearly, for scales $r < \eta_\omega$ the structure function shows again the Taylor expansion behavior $D_2^{(B)}(r) = (\epsilon_B/2\eta) r^2$ as stated in Eq. (14). The larger the scales the more dominant the constant first term in Eq. (16), which is proportional to the magnetic Prandtl number, leading to a saturation at a constant value $D_2^{(B)}(\infty) = 2\epsilon_\psi/\eta$ for large distances, i.e. where $D_2^{(B)} \sim r^0$. The crossover between both scaling regimes is relatively sharp and shifted towards smaller r for growing values of Pr_m. We could not observe an intermediate algebraic scaling between both ranges.

The spatial correlations in the magnetic field are subdominant in $D_2^{(B)}(r)$ for scales $r \gtrsim \eta_\omega$, but show up in the correlation function $C_2^{(B)}(r)$: an algebraic scaling $D_2^{(\psi)}(r) \sim r^\alpha$ corresponds to $C_2^{(B)}(r) \sim r^{\alpha-2}$. The results for the correlation function, derived using (17), are shown in Fig. 4 for different values of Pr_m and α. In the logarithmic plot the algebraic decay of the correlation for all discussed parameter sets is clearly visible in particular, a $r^{-4/3}$–decay is found in regions where $D_2^{(\psi)}(r) \sim r^{2/3}$ (see also Fig. 2). The correlations decay very fast when

the magnetic flux is advected passively with the turbulent velocity field.

The results show an anticorrelation of the magnetic fields, i.e. $C_2^{(B)} < 0$. It is observed near the crossover from $D_2^{(\psi)} \sim r^2$ to $D_2^{(\psi)} \sim r^0$, i.e. near the transition from the viscous regime to the Batchelor plateau. This follows also analytically within the Batchelor parametrization [24] of $D_2^{(\psi)}(r)$ by setting

$$D_2^{(\psi)}(r) = \frac{r^2}{1 + a_2 r^2} \,, \tag{26}$$

which approximates such a crossover very well. Equation (17) then gives

$$\frac{1}{r}\partial_r(r\partial_r D_2^{(\psi)}(r)) = 4\frac{1 - a_2 r^2}{(1 + a_2 r^2)^3} \,. \tag{27}$$

With $a_2 > 0$ and $r \geq 0$ we find negative values of (27) for $r > (a_2)^{-1/2}$. It can be shown that a crossover of $D_2^{(\psi)}(r)$ from r^α to r^β with $0 \leq \beta \leq \alpha \leq 2$ gives negative values in (27) and thus anticorrelation of the magnetic field at all when in addition the constraint $\beta < \alpha/5$ is satisfied. This is consistent with our results for extremely small magnetic Prandtl numbers where no anticorrelation is observed. Here, the quadratic scaling with r changes directly to an $r^{2/3}$–scaling (see Figs. 2 and 4), and the intermediate Batchelor plateau is not present.

The anticorrelation in the normalized correlation function is magnified in Fig. 5 for values of Pr_m reaching from 10^{-5} to 10^3. The negative contributions vanish for sufficiently low Pr_m where the Batchelor plateau is supressed (see the cases $Pr_m = 10^{-4}, 10^{-5}$). On the other hand we observe a nearly constant value $\min\left(C_2^{(B)}\right) \simeq -0.0375\epsilon_\psi/\eta$ for the larger values of the magnetic Prandtl number.

The origin of this anticorrelation presumably lies in the advection of ψ in turbulent flow structures and the formation of strongly filamented flux sheets (and thus current sheets) in which the magnetic energy is stored. The minimal sheet width δ_{CS} can be determined by the balance between the advection and the diffusion term of (10), giving

$$\frac{U_l}{l}\psi \simeq \eta\frac{\psi}{\delta_{CS}^2} \,. \tag{28}$$

By taking $U_l/l = \epsilon_\omega^{1/3}$ as the typical strain rate we end up with

$$\delta_{CS} \simeq \eta_\omega Pr_m^{-1/2} \,. \tag{29}$$

This Pr_m scaling is also found in the position of the minimum, so that the anticorrelation is due to layers with opposite orientations of magnetic fields. The saturation of the anticorrelation in Fig. 5 suggests that the ratio of regions with perfect parallel alingment and deviations, say due to folds or modulations in thickness, stays the same, independent of magnetic Prandtl number.

The relation (29) can also be derived by means of (22). Assuming the subdominance of the $\alpha Pr_m r^2$ term, we can ask when the last term under the square root in (22) will exceed unity. By requiring a smooth flow in the viscous subrange, i.e. setting $D_\parallel \sim r^2$, we get the same Pr_m dependence as in (29).

V. FULL MHD BEYOND THE KINEMATIC REGIME

In the following the results of the kinematic approach are compared with direct numerical simulations [25] as well as integrations of spectral transfer equations within closure models [26], both at $Pr_m = 1$ and with a kinetic energy about three orders of magnitude larger than the magnetic energy. This provides insights into the feedback of the magnetic field on the flow via the Lorentz force density. The question is whether the phenomena seen in the kinematic case, in particular the anticorrelation, will still be present.

Both numerical experiments support the existence of a Kolmogorov-type scaling for the spectrum of the mean square magnetic potential, $A(k) \sim k^{-7/3}$ for $k < k_f$, in the inverse mean square flux cascade range. The Alfvén effect causing an equipartion between kinetic and magnetic energy is subdominant. The spectral closure suggests $A(k) \sim k^{-7/2}$ for the direct energy cascade range $k > k_f$. We start with a corresponding model spectrum for the amplitudes $\langle|\psi_\mathbf{k}|^2\rangle$ (see Fig. 6(a))

$$\langle|\psi_\mathbf{k}|^2\rangle \sim \begin{cases} k_f^{-7/6}k_1^{-13/3}k^3 & : \quad \frac{2\pi}{L} \leq k \leq k_1, \\ k_f^{-7/6}k^{-4/3} & : \quad k_1 < k \leq k_f, \\ k^{-5/2} & : \quad k_f < k \leq k_d, \\ k^{-5/2}\exp\left[-\left(\frac{k-k_d}{k_d}\right)^2\right] & : \quad k_d < k \,, \end{cases} \tag{30}$$

where $k_d \sim \eta_d^{-1}$ is the wave number at the viscous cut off. The structure function is calculated as in section III:

$$D_2^{(\psi)}(r) = 2\sum_k \langle|\psi_\mathbf{k}|^2\rangle\,(1 - \mathrm{J}_0(kr)) \,. \tag{31}$$

The resulting structure function is shown in panel (b) of Fig. 6. The inset gives $\zeta_2^{(\psi)}$ vs. r measured in units of η_d. Consequently $D_2^{(\psi)}(r)$ has to be taken now in units

of $\epsilon_\psi \epsilon^{-1/2} \nu^{1/2}$. The r^2–scaling for $r < \eta_d$ is followed by a range with $\zeta_2^{(\psi)} \approx \frac{4}{3}$ for $r > \eta_d$, which seems to be connected with the extended inverse cascade of the mean square magnetic potential. Again structure function and correlation function are calculated by means of (16) and (17), respectively. Consistency was checked by calculating $D_2^{(B)}(r)$ directly via $\langle |\mathbf{B_k}|^2 \rangle \sim k^2 \langle |\psi_\mathbf{k}|^2 \rangle$ using a relation equivalent to (31). The function $D_2^{(B)}(r)$ is shown in Fig. 3 as the dash-dotted line. We see that it reaches the constant saturation state for scales r larger than in the kinematic case. The differences between the kinematic and full dynamic situation are more pronounced in the correlation functions [see Fig. 6(c)]. The correlations decay slower with respect to r, following now a $r^{-2/3}$–law.

Besides the different scalings we note that the anticorrelation has disappeared. In the full dynamic case the magnetic field itself would prohibit the build-up of elongated current sheets (flux sheets) due to its feedback via the Lorentz force density

$$\mathbf{f}_L = -\nabla \left(\frac{B^2}{2\mu_0} \right) + \frac{1}{\mu_0} (\mathbf{B} \cdot \nabla) \mathbf{B} \; . \tag{32}$$

The current sheets, if formed, become sensitive to several resistive instabilities such as the spontaneous growth of the tearing mode, [27–29] where the stored magnetic energy can be released into the plasma flow by means of magnetic reconnection. In this process the Lorentz force density causes the plasma acceleration due to reconnected magnetic flux and prevents a further steepening of flux up to the dissipative scales. Thus in addition to the condition $M > R_m$ the Reynolds number R has to be sufficiently low to avoid resistive MHD instabilities. It was found that the onset of the tearing mode instability is determined by the Hartmann number $Ha = \sqrt{R_m R} = R\sqrt{Pr_m}$ and the width δ_{CS}. [30,31]

VI. SUMMARY

Our findings for the magnetic structure function as well as the corresponding correlation function in a two-dimensional MHD system can be summarized as follows.

(1) For the kinematic regime of two-dimensional MHD turbulence ($M \gg 1$), the magnetic flux function ψ can be treated as a passive scalar advected in a turbulent flow. By means of the geometric scaling theory the second order structure function $D_2^{(\psi)}(r)$ was calculated over a wide range of scales r and of magnetic Prandtl numbers Pr_m. For this case a rather complete analysis is now possible by means of Eq. (22).

(2) The second order magnetic structure function $D_2^{(B)}(r)$ and the corresponding magnetic correlation function $C_2^{(B)}(r)$ were calculated by exact analytical relations from $D_2^{(\psi)}(r)$. The larger Pr_m the smaller the scale r where the structure function reaches the constant saturation. The correlation function decays fast with $r^{-4/3}$ and shows an anticorrelation. The latter is connected with the transition to the Batchelor regime and can be associated with an attempt of the system to concentrate its magnetic energy in strongly filamented structures. This process is limited by the finite resistivity η. The anticorrelation minimum was found to be independent of the magnetic Prandtl number.

(3) The results for the kinematic approach were compared to results in the dynamic regime $M < R_m$. The magnetic field correlations decay with $r^{-2/3}$, i.e. slower than for the kinematic case. This can be explained by the feedback of the magnetic field on the flow which prohibits the build-up of strongly filamented, elongated current sheets on small scales. Therefore no anticorrelation was detected.

While the discussion in this paper was limited to the 2-D case, a weak field regime without dynamo can also be identified in three dimensions. In the experiments of Odier *et al.* [32] a scaling of the magnetic field was observed that is very close to what one expects for a passive scalar. Thus the stretching of the magnetic field does not seem to have a pronounced effect on the structure function. Further investigations of this point seem worthwhile.

ACKNOWLEDGMENTS

Fruitful discussions with H. Fuchs and K.-H. Rädler are gratefully acknowledged.

APPENDIX A: DERIVATION OF EQUATION (16)

The second order structure function $D_2^{(B)}(r)$ was decomposed in Eq. (13) into (the sum convention is used)

$$\begin{aligned} D_2^{(B)}(r) &= 2\langle B_i^2 \rangle - 2C_2^{(B)}(r), \\ &= 2R_{ii}^{(B)}(0) - 2R_{ii}^{(B)}(\mathbf{r}), \end{aligned} \tag{A1}$$

where $R_{ij}^{(B)}(\mathbf{r}) = \langle B_i(\mathbf{x}) B_j(\mathbf{x}+\mathbf{r}) \rangle$ is the static magnetic field correlation tensor. A detailed analysis of the properties of $R_{ij}^{(B)}(\mathbf{r})$ can be found in Oughton *et al.* [33] Next we apply $\epsilon_{ijk}\epsilon_{ilm} = (\delta_{jl}\delta_{km} - \delta_{jm}\delta_{kl})$ for $\mathbf{B} = \nabla \times \mathbf{A}$ in the autocorrelated part and get

$$\begin{aligned} B_i^2 &= \epsilon_{ijk} \partial_{x_j} A_k \epsilon_{ilm} \partial_{x_l} A_m, \\ &= (\partial_{x_j} A_m)^2 - (\partial_{x_j} A_m \partial_{x_m} A_j). \end{aligned} \tag{A2}$$

The statistical average gives

$$\langle B_i^2 \rangle = \langle (\partial_{x_j} A_m)^2 \rangle = \frac{\epsilon_A}{\eta}, \tag{A3}$$

where the second term vanishes due to homogeneity. The trace of the magnetic field correlation tensor can be decomposed in a similar way by using [34]

$$\langle B_i(\mathbf{x})B_i(\mathbf{x}+\mathbf{r})\rangle = -\epsilon_{ijk}\epsilon_{ilm}\partial_{r_j}\partial_{r_l}R^{(A)}_{km}(\mathbf{r}),$$
$$= -\partial^2_{r_l}R^{(A)}_{mm}(\mathbf{r}),$$
$$= \frac{1}{2}\Delta D_2^{(A)}(r). \qquad \text{(A4)}$$

For the derivation the Coloumb gauge $\nabla \cdot \mathbf{A} = 0$ has to be taken. Finally we get in 3-D

$$D_2^{(B)}(r) = 2\frac{\epsilon_A}{\eta} - \Delta D_2^{(A)}(r), \qquad \text{(A5)}$$

and it follows in 2-D with $\mathbf{A} = (0, 0, \psi(x, y))$ Eq. (16)

$$D_2^{(B)}(r) = 2\frac{\epsilon_\psi}{\eta} - \Delta D_2^{(\psi)}(r). \qquad \text{(A6)}$$

The dimensionless form of (16), $D_2^{(B)} = 2Pr_m - \Delta D_2^{(\psi)}$, was solved numerically over a large range of scales r. We substitute the Laplacian in the following way

$$\Delta D_2^{(\psi)} = \frac{1}{r}\partial_r\left[r\partial_r D_2^{(\psi)}\right],$$
$$= \frac{D_2^{(\psi)}}{r^2}\left[(\partial_{\ln r} g)^2 + \partial^2_{\ln r} g\right]. \qquad \text{(A7)}$$

Here $g(\ln r) = \ln D_2^{(\psi)}(r)$ was set. The function g is approximated with cubic splines in a least square fit using the Numerical Algorithms Group (NAG) library.

[1] D. Biskamp, *Nonlinear Magnetohydrodynamics* (Cambridge University Press, Cambridge, England, 1993).
[2] E. Marsch, C.-Y. Tu, and H. Rosenbauer, Ann. Geophysicae **14**, 259 (1996).
[3] J. Kuijpers, "Flares in Accretion Discs", in *Coronal Magnetic Energy Releases*, A. O. Benz and A. Krüger, eds. (Lecture Notes in Physics, Springer, Heidelberg, 1995), Vol. 444, pp. 135-158.
[4] Ya. B. Zeldovich and A. A. Ruzmaikin, Sov. Phys. JETP **51**, 493 (1980).
[5] D. Biskamp and H. Welter, Phys. Fluids B **2**, 1787 (1990).
[6] F. Cattaneo and S. I. Vainshtein, Astrophys. J. **376**, L21 (1991).
[7] P. Constantin and I. Procaccia, Phys. Rev. E **47**, 3307 (1993); P. Constantin and I. Procaccia, Nonlinearity **7**, 1045 (1994).
[8] I. Procaccia and P. Constantin, Europhys. Lett. **22**, 689 (1993).
[9] B. Eckhardt and J. Schumacher, "Structure function of passive scalars in two-dimensional turbulence", submitted to Phys. Rev. E (1998).
[10] Ya. B. Zeldovich, *Magnetic Fields in Astrophysics* (Gordon and Breach, New York, U.S.A., 1983).
[11] D. Biskamp, Europhys. Lett. **21**, 563 (1993).
[12] R. Grauer and C. Marliani, Phys. Plasmas **2**, 41 (1995).
[13] S. Grossmann and P. Mertens, Z. Phys. B **88**, 105 (1992).
[14] J. Paret and P.Tabeling, Phys. Rev. Lett. **79**, 4162 (1997); J. Paret and P.Tabeling, Phys. Fluids **10**, 3126 (1998).
[15] M. A. Rutgers, Phys. Rev. Lett. **81**, 2244 (1998).
[16] U. Frisch and P. L. Sulem, Phys. Fluids **27**, 1921 (1984).
[17] L. M. Smith and V. Yakhot, Phys. Rev. Lett. **71**, 352 (1993).
[18] R. Benzi, C. Paladin, S. Patarnello, P. Santangelo, and A. Vulpiani, J. Phys. A **19**, 3771 (1986).
[19] J. Paret, M.-C. Jullien, and P. Tabeling, "Vorticity Statistics in the two-dimensional enstrophy cascade", submitted to Phys. Rev. Lett. (1999).
[20] A. Babiano, C. Basdevant, B. Legras, and R. Sadourny, J. Fluid Mech. **183**, 379 (1987).
[21] C. Basdevant and T. Philipovitch, Physica D **37**, 17 (1994).
[22] G. K. Batchelor, J. Fluid Mech. **5**, 113 (1959).
[23] A. M. Obukhov, Izv. Akad. Nauk SSSR, Ser. Geog. Geofiz. **13**, 58 (1949); S. Corrsin, J. Appl. Phys. **22**, 469 (1951).
[24] G. K. Batchelor, Proc. Camb. Phil. Soc. **47**, 359 (1951).
[25] D. Biskamp and U. Bremer, Phys. Rev. Lett **72**, 3819 (1993).
[26] A. Pouquet, U. Frisch, and J. Léorat, J. Fluid Mech. **77**, 321 (1976); A. Pouquet, J. Fluid Mech. **88**, 1 (1978).
[27] H. P. Furth, J. Killeen, and M. N. Rosenbluth, Phys. Fluids **6**, 459 (1963).
[28] W. H. Matthaeus and S. L. Lamkin, Phys. Fluids **29**, 2513 (1986).
[29] H. Politano, A. Pouquet, and P. L. Sulem, Phys. Fluids B **1**, 2330 (1989).
[30] R. B. Dahlburg, T. A. Zang, D. Montgomery, and M. Y. Hussaini, Proc. Natl. Acad. Sci. USA **80**, 5798 (1983).
[31] N. Seehafer and J. Schumacher, Phys. Plasmas **5**, 2363 (1998).
[32] P. Odier, J.-F. Pinton, and S. Fauve, Phys. Rev. E **58**, 7397 (1998).
[33] S. Oughton, K.-H. Rädler, and W. H. Matthaeus, Phys. Rev. E **56**, 2875 (1997).
[34] A. S. Monin and A. M. Yaglom, *Statistical Fluid Mechanics*, (MIT Press, Cambridge, Massachusetts, 1975).

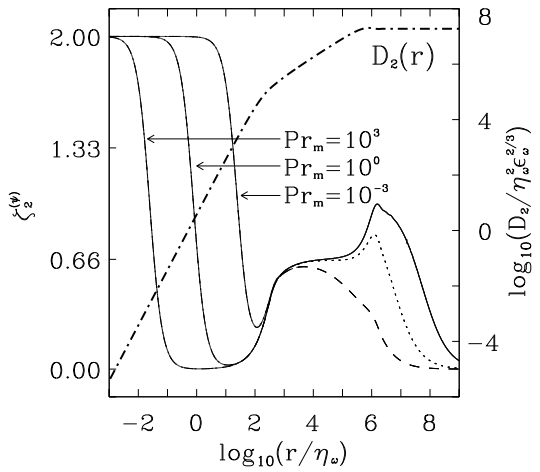

FIG. 1. Velocity structure function $D_2(r)$ (dash-dotted line) and the scaling exponent $\zeta_2^{(\psi)}(r)$ of the structure function $D_2^{(\psi)}(r)$ for three values of the prefactor $\alpha = \epsilon_\psi \epsilon_\omega^{-1/3} \psi_{r.m.s.}^{-2}$ and three values of the magnetic Prandtl number. The solid line stands for $\alpha = 10^{-4}$, the dotted for $\alpha = 10^{-3}$, and the dashed line for $\alpha = 10^{-2}$. For small distances r the α-dependence is subdominant and thus the curves for the same magnetic Prandtl number coincide.

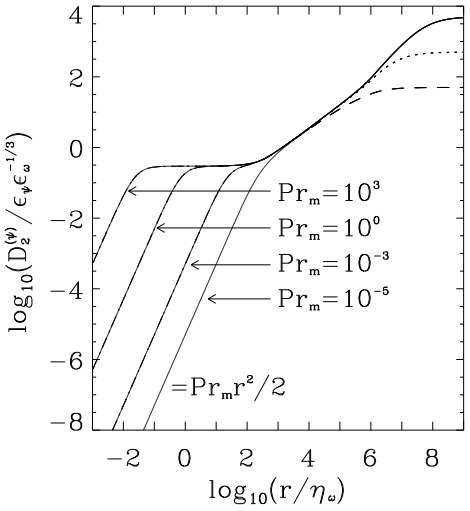

FIG. 2. Structure function $D_2^{(\psi)}(r)$ with respect to r for α as in Fig. 1. Additionally the structure function for $Pr_m = 10^{-5}$ for $\alpha = 10^{-4}$ is shown which has no Batchelor plateau. All linestyles are chosen as in Fig. 1.

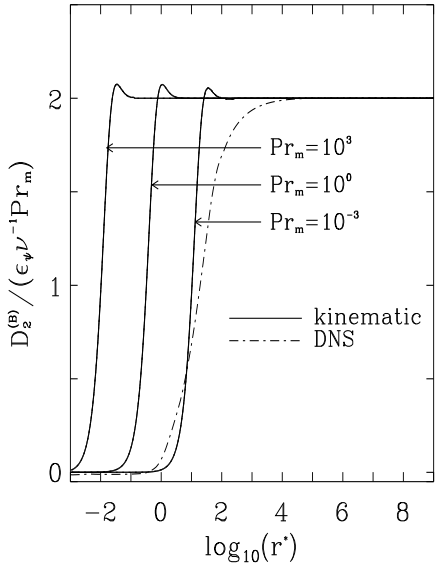

FIG. 3. Normalized structure function $D_2^{(B)}(r)/(\epsilon_\psi \nu^{-1} Pr_m)$ vs. $r^* = r/\eta_\omega$ for α as in Fig. 1. The curves for the different values of α, but the same Pr_m, coincide. Additionally, $D_2^{(B)}(r)/(\epsilon_\psi \nu^{-1})$ vs. $r^* = r/\eta_d$ calculated from direct numerical simulations (DNS) at $Pr_m = 1$ is plotted as a dash-dotted line.

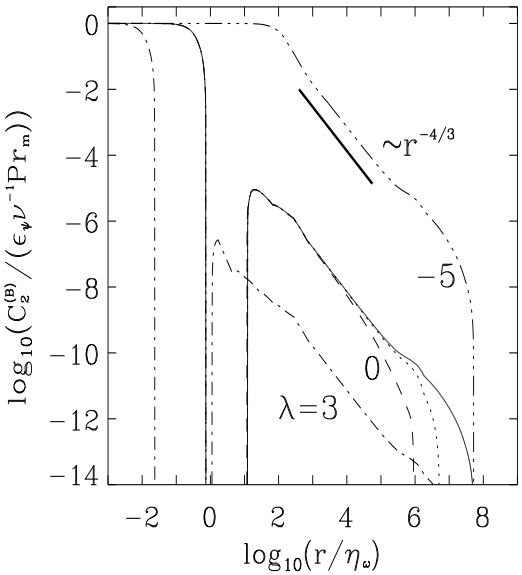

FIG. 4. Normalized magnetic correlation function $C_2^{(B)}(r)/(\epsilon_\psi \nu^{-1} Pr_m)$ vs. r/η_ω for $Pr_m = 10^\lambda$. For $Pr_m = 1$ the correlation functions are shown for the three values of α as in Fig. 1 using the same linestyles as therein.

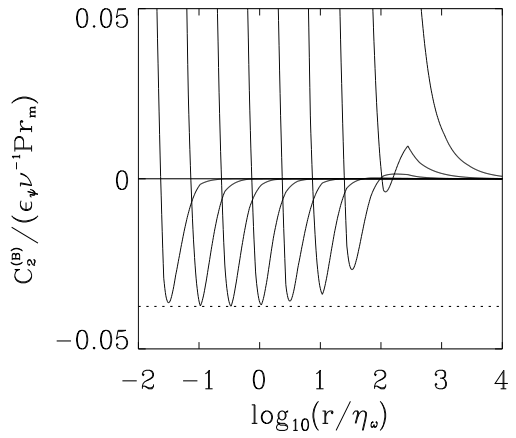

FIG. 5. Anticorrelated part of $C_2^{(B)}(r)$ where the magnetic Prandtl number Pr_m decreases by a factor 10 from 10^3 for the left most curve to 10^{-5} at the right end. The parameter α was set to 10^{-4}.

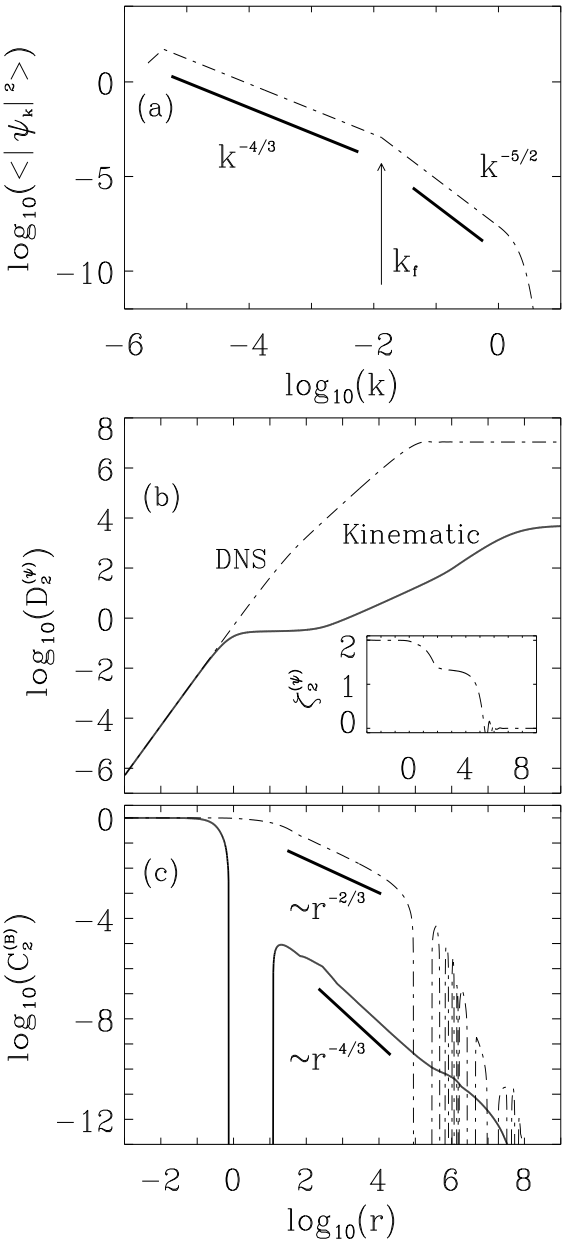

FIG. 6. (a): Mean square potential spectrum $\langle|\psi_{\mathbf{k}}|^2\rangle$ vs. k resulting from full MHD simulation results. The extension of the two cascade ranges is identical to those of the velocity input spectrum for the kinematic calculations. (b): Corresponding structure function $D_2^{(\psi)}(r)$ vs. r plotted with the same linestyle as (a) and compared with its kinematic counterpart for $\alpha = 10^{-4}$. The inset shows the corresponding $\zeta_2^{(\psi)}(r)$. (c): Both magnetic correlation functions are plotted corresponding to (b). All quantities are expressed in characteristical units and $Pr_m = 1$ was taken.